Journal of Solid State Chemistry **162,** 113–121 (2001)
doi:10.1006/jssc.2001.9363, available online at http://www.idealibrary.com on IDEAL®

Synthesis and Characterization of New Strontium Iron(II) Phosphates, $SrFe_2(PO_4)_2$ and $Sr_9Fe_{1.5}(PO_4)_7$

A. A. Belik, B. I. Lazoryak,[1] K. V. Pokholok, and T. P. Terekhina

Department of Chemistry, Moscow State University, 119899 Moscow, Russia
E-mail: lazoryak@tech.chem.msu.ru

and

I. A. Leonidov, E. B. Mitberg, V. V. Karelina, and D. G. Kellerman

Institute of Solid State Chemistry Ural Branch, Russian Academy of Sciences, Pervomayskaia 91, GSP-145, 620219 Yekaterinburg, Russia

Received May 1, 2001; in revised form August 13, 2001; accepted August 17, 2001

New strontium iron(II) orthophosphates, $SrFe_2(PO_4)_2$ and $Sr_9Fe_{1.5}(PO_4)_7$, were synthesized by the solid state method at 1170 K. They were characterized by X-ray powder diffraction, thermal analysis in air, magnetic susceptibility, and the IR and Mössbauer spectroscopy methods. Mössbauer spectroscopy confirmed the presence of only Fe^{2+} cations in both compounds. $SrFe_2(PO_4)_2$ crystallizes in a monoclinic system with $a =$ 10.5376(7) Å, $b = 6.8529(4)$ Å, $c = 9.3658(6)$ Å, $\beta =$ 109.498(5)°. The crystal structure of $Sr_9Fe_{1.5}(PO_4)_7$ was refined by the Rietveld method: space group $R\bar{3}m$; $Z = 3$; $a = 10.6102(1)$ Å, $c = 19.7135(1)$ Å with $R_{wp} = 3.00\%$ ($S = 1.51$), $R_p = 2.35\%$, $R_B = 3.44\%$, $R_F = 1.72\%$. A second-harmonic-generation study showed that the structures of these two compounds have a center of symmetry. The crystal structure of $Sr_9Fe_{1.5}(PO_4)_7$ is related to that of β-$Ca_3(PO_4)_2$ and α-$Sr_3(PO_4)_2$, but is topologically more similar to that of β-$Ca_3(PO_4)_2$. Tetrahedra $P1O_4$ and strontium cations in the $M3$ sites are disordered in the structure of $Sr_9Fe_{1.5}(PO_4)_7$. The octahedral $M5$ site is fully occupied and the $M4$ site is quarter-occupied by iron cations. $SrFe_2(PO_4)_2$ and $Sr_9Fe_{1.5}(PO_4)_7$ are stable in air up to 750 and 810 K, respectively. © 2001 Academic Press

Key Words: **phosphate; iron; strontium; crystal structure; Rietveld method; Mössbauer spectroscopy; IR spectroscopy; magnetic susceptibility.**

1. INTRODUCTION

Orthophosphates $A_3(PO_4)_2$ (A^{2+} = Mg, Ca, Sr, Ba, Cd, and Zn) with different substitutions have been extensively studied for their applications as luminescence materials (1–5). The $M_3(PO_4)_2$–$Sr_3(PO_4)_2$ systems were investigated for M = Ca, Mg, Zn (1), and Cd (2). Sarver *et al.* (1) have reported the existence of solid solutions $Sr_{3-x}Mg_x(PO_4)_2$ ($0.27 \le x \le 1.08$ at 1273 K) and $Sr_{3-x}Zn_x(PO_4)_2$ ($0.27 \le x \le 0.81$ at 1298 K), which are isotypic with β-$Sr_3(PO_4)_2$, and the compounds $SrMg_2(PO_4)_2$ and β-$SrZn_2(PO_4)_2$ with unknown crystal lattices. β-$Sr_3(PO_4)_2$ was supposed to be isotypic with β-$Ca_3(PO_4)_2$ (1). Looney and Brown (2) have found the solid solutions $Sr_{3-x}Cd_x(PO_4)_2$ ($0.36 \le x \le 0.63$ at 1273 K) with the β-$Sr_3(PO_4)_2$ structure type and the compound $SrCd_2(PO_4)_2$ with unknown crystal lattice. Crystal structures have been determined for α-$SrZn_2(PO_4)_2$ (6), $SrNi_2(PO_4)_2$ (7), $Sr_2Ni(PO_4)_2$ (8), $SrCo_2(PO_4)_2$ (9), $Sr_2Co(PO_4)_2$ (10), $SrMn_2(PO_4)_2$ (11), $Sr_3Cu_3(PO_4)_4$ (12, 13), $Sr_{9.1}Cu_{1.4}(PO_4)_7$ (13), and $Sr_2Cu(PO_4)_2$ (13). The compound $Sr_{1.9}Cu_{4.1}(PO_4)_4$ crystallizing in orthorhombic system has also been described (13).

Iron phosphates have shown a rich structural chemistry. In the system Sr–Fe–P–O the compounds $SrFe_3(PO_4)_3$ (14), $SrFe_3(P_2O_7)_2$ (15), $SrFe_2(P_2O_7)_2$ (16), and $SrFeP_2O_7$ (17) have been obtained and characterized. Other strontium iron phosphates have also been described, for example, $SrFe_3(PO_4)_3(HPO_4)$ (18) and $Sr_2Fe(PO_4)_2(H_2PO_4)$ (19). In this paper, we report the synthesis and X-ray powder diffraction, thermal analysis, magnetic susceptibility, IR and Mössbauer spectroscopy studies of new orthophosphates in the $Fe_3(PO_4)_2$–$Sr_3(PO_4)_2$ system, $SrFe_2(PO_4)_2$ and $Sr_9Fe_{1.5}(PO_4)_7$.

2. EXPERIMENTAL

Specimens $SrFe_2(PO_4)_2$, $Sr_2Fe(PO_4)_2$, $Sr_9Fe_{1.5}(PO_4)_7$, and $Sr_{9.5}Fe(PO_4)_7$ were synthesized from stoichiometric mixtures of $Sr_3(PO_4)_2$, $FePO_4$, and Fe (99.999%) by the solid state method at 1170–1190 K (240 h with one intermediate grinding) under Ar in alumina crucibles. After annealing the samples were cooled in a furnace. The obtained specimens were white in color. $Sr_3(PO_4)_2$ and $FePO_4$

[1] To whom correspondence should be addressed.

0022-4596/01 $35.00

were synthesized from stoichiometric mixtures of $SrCO_3$ (99.999%), Fe_2O_3 (99.8%), and $NH_4H_2PO_4$ (99.999%) by the solid state method at 1270 K for 100 h.

X-ray powder diffraction (XRD) measurements were performed at room temperature with a Siemens D500 Bragg–Brentano-type powder diffractometer equipped with an incident-beam quartz monochromator to obtain Cu$K\alpha_1$ radiation ($\lambda = 1.5406$ Å) and a Braun position-sensitive detector and operated at 30 kV and 30 mA, respectively. Silicon was used as an external standard. For phase analysis XRD data were collected between $2\theta = 10^\circ$ and 60° with a step interval of 0.02°. For the samples $SrFe_2(PO_4)_2$ and $Sr_9Fe_{1.5}(PO_4)_7$, XRD data were collected in the range $2\theta = 8^\circ$–140°. The structure refinement of $Sr_9Fe_{1.5}(PO_4)_7$ was carried out by the Rietveld method (20) with RIETAN-2000 (21, 22). The split pseudo-Voigt function of Toraya (23) was fitted to each profile and a ninth-order Legendre polynomial to the background. Partial profile relaxation (21, 22) was applied to the reflection 012, 110, 015, 122, 205, 220, 404, 045, and 324 to improve fits in these reflections at the last stages of the structure refinement. A preferred orientation was not observed in the XRD pattern of $Sr_9Fe_{1.5}(PO_4)_7$. Scattering factors for Sr^{2+}, Fe^{2+}, P, and O^- were used (24). Standard deviations were estimated by the conventional method.

The thermal stability of $SrFe_2(PO_4)_2$ and $Sr_9Fe_{1.5}(PO_4)_7$ in air was examined with the instrument TG-DTA-92 (Setaram). The specimens ($\sim$100 mg) were heated from room temperature to 1270 K in air at the rate 2.6 K/min.

IR spectra were recorded on a Nicolet Magna-750 Fourier spectrometer in the wavenumber range of 400–4000 cm^{-1} using the KBr pellet technique.

Iron-57 Mössbauer spectra were taken using a constant acceleration Mössbauer spectrometer coupled with a 1024-multichannel analyzer and a ^{57}Co/Rh source kept at RT. All isomer shift values (δ) given hereafter are made in reference to α-Fe. Experimental data were resolved into symmetric quadrupole doublets with Lorentzian lineshapes using an iterative least-squares fitting program.

Magnetic susceptibility data were recorded from powder samples using a Faraday-type magnetometer in the temperature range 300–920 K.

The second-harmonic-generation response of thin powder samples was measured in the reflection mode. A Q-switch pulsed Nd:YAG laser operating at 1064 nm with a 6.25-Hz repetition rate and a 12-ns pulse width was used as radiation source. The average power incident on the reflector was 0.5 MW. Powdered crystalline α-SiO_2 was used as a standard sample.

3. RESULTS AND DISCUSSION

3.1. Phase Analysis

Table 1 presents the results of phase analysis for the synthesized samples. The samples $SrFe_2(PO_4)_2$ and $Sr_9Fe_{1.5}(PO_4)_7$ were single phased. The XRD pattern of $SrFe_2(PO_4)_2$ was indexed using the TREOR90 program (25): monoclinic system; $a = 10.5376(7)$ Å, $b = 6.8529(4)$ Å, $c = 9.3658(6)$ Å, $\beta = 109.498(5)^\circ$ (figures of merit: $M_{20} = 23.1$, $F_{30} = 47.8$ (0.0116, 54); indexing was made using 122 reflections in the range $2\theta = 8^\circ$–68°). Index results for $SrFe_2(PO_4)_2$ will be published in the Powder Diffraction File. The compound $Sr_9Fe_{1.5}(PO_4)_7$ crystallizes in trigonal symmetry with $a = 10.6102(1)$ Å and $c = 19.7135(1)$ Å and was found to have the β-$Sr_3(PO_4)_2$ structure type (1, 2) and, consequently, to be related to β-$Ca_3(PO_4)_2$ (26) or mineral whitlockite (27).

The weight fraction of α-$Sr_3(PO_4)_2$ (28) in the $Sr_{9.5}Fe(PO_4)_7$ sample calculated by the RIETAN-2000 program was 15.2%, which gave the composition of the β-$Sr_3(PO_4)_2$-type phase as $Sr_{9.32}Fe_{1.18}(PO_4)_7$. Thus, in the $Fe_3(PO_4)_2$–$Sr_3(PO_4)_2$ system there exist the solid solutions $Sr_{3-x}Fe_x(PO_4)_2$ with the β-$Sr_3(PO_4)_2$ structure type and the compound $SrFe_2(PO_4)_2$, as in the systems $M_3(PO_4)_2$–$Sr_3(PO_4)_2$ with M = Mg, Zn (1), and Cd (2). Note that the $Cu_3(PO_4)_2$–$Sr_3(PO_4)_2$ system has four binary compounds (13), $Sr_{1.9}Cu_{4.1}(PO_4)_4$, $Sr_3Cu_3(PO_4)_4$, $Sr_2Cu(PO_4)_2$, and $Sr_{9.1}Cu_{1.4}(PO_4)_7$, and the $Ni_3(PO_4)_2$–$Sr_3(PO_4)_2$ and $Co_3(PO_4)_2$–$Sr_3(PO_4)_2$ systems have three binary compounds, $SrM_2(PO_4)_2$ (7, 9), $Sr_2M(PO_4)_2$ (8, 10), and $Sr_{9+x}M_{1.5-x}(PO_4)_7$ (M = Co and Ni) (29). The boundaries of the solid solutions $Sr_{3-x}Fe_x(PO_4)_2$ with the β-$Sr_3(PO_4)_2$ structure are at least $0.34 \le x \le 0.43$. The extension of the solid solutions $Sr_{3-x}M_x(PO_4)_2$ with M = Fe is narrower than for M = Mg and Zn, but comparable with M = Ni, Co, and Mn (Table 2). Each system $Sr_{3-x}M_x(PO_4)_2$ (M = Mg, Mn, Fe, Co, Ni, Cu, Zn, and Cd) has its own range of solid solutions with the β-$Sr_3(PO_4)_2$ structure.

3.2. Physical Characterization

The Mössbauer spectra of $SrFe_2(PO_4)_2$ and $Sr_9Fe_{1.5}(PO_4)_7$ are shown in Fig. 1 and the hyperfine parameters corresponding to the fits shown in this figure are given in Table 3. The isomer shifts obtained are characteristic of

TABLE 1
Results of Phase Analysis for Samples in the Study

Total composition of the sample	Phase composition
$SrFe_2(PO_4)_2$	Single phase
$Sr_2Fe(PO_4)_2$	β-phase ($a = 10.5965(5)$ Å and $c = 19.7224(6)$ Å) + unknown phases
$Sr_9Fe_{1.5}(PO_4)_7$	Single phase (β-phase)
$Sr_{9.5}Fe(PO_4)_7$	β-phase ($a = 10.6510(5)$ Å and $c = 19.6749(5)$ Å) + α-$Sr_3(PO_4)_2$

Note. β-phase: a β-$Sr_3(PO_4)_2$-type phase.

TABLE 2
Ranges of Solid Solutions with the β-$Sr_3(PO_4)_2$ Structure in the $Sr_{3-x}M_x(PO_4)_2$ Systems

M	Solid solution extension	Ref.
Mg	$0.27 \le x \le 1.08$	1
Mn	$0.33 \le x \le 0.41$	29
Fe	$0.34 \le x \le 0.43$	This work
Co	$0.35 \le x \le 0.43$	29
Ni	$0.32 \le x \le 0.39$	29
Cu	$0.39 \le x \le 0.41$	13, 29
Zn	$0.27 \le x \le 0.81$	1
Cd	$0.36 \le x \le 0.63$	2, 29

TABLE 3
Parameters of Mössbauer Spectra for $SrFe_2(PO_4)_2$ and $Sr_9Fe_{1.5}(PO_4)_7$

Compound	δ^a (mm/s)	$\Delta E_Q{}^b$ (mm/s)	Γ^c (mm/s)	S^d (%)
$SrFe_2(PO_4)_2$, 300 K	1.27(1)	2.60(1)	0.27(1)	45(1)
	1.27(1)	2.93(1)	0.27	55(1)
$Sr_9Fe_{1.5}(PO_4)_7$, 300 K	1.26(1)	1.90(1)	0.35(1)	32(1)
	1.23(1)	1.45(1)	0.35	34(1)
	1.26(1)	1.03(1)	0.35	34(1)
$Sr_9Fe_{1.5}(PO_4)_7$, 80 K	1.38(1)	2.62(1)	0.39(1)	41(1)
	1.28(1)	2.17(1)	0.39	30(1)
	1.37(1)	1.69(1)	0.39	29(1)

Note. Γ values were constrained.
[a] Isomer shift.
[b] Quadrupole splitting.
[c] Full-width at half-maximum.
[d] Area.

Fe(II). The usual range of isomer shifts in oxide is 1.03–1.28 mm/s for Fe(II) in six-coordination (30). The Mössbauer spectra of $Sr_9Fe_{1.5}(PO_4)_7$ could be satisfactorily fitted at least by three doublets. When the spectra were fitted by two doublets (as may be expected from structural information, see below), the fitting was not good or the isomer shift of one doublet was too large (1.46 mm/s at 300 K and 1.57 mm/s at 80 K). Mössbauer spectroscopy indicated that the structure of $Sr_9Fe_{1.5}(PO_4)_7$ has more than two types of oxygen-surrounding iron cations. This may be associated with the disordered character of the structure of $Sr_9Fe_{1.5}(PO_4)_7$ revealed by the structure refinement. The Mössbauer spectrum of $SrFe_2(PO_4)_2$ presented one doublet ($\delta = 1.27(1)$ mm/s, $\Delta E_Q = 2.78(1)$ mm/s, $\Gamma = 0.37(1)$ mm/s), but the width at half-maximum was slightly different for doublet components (0.39 and 0.36 mm/s). Also the spectrum of $SrFe_2(PO_4)_2$ was fitted much better by two doublets (Fig. 1a, Table 3).

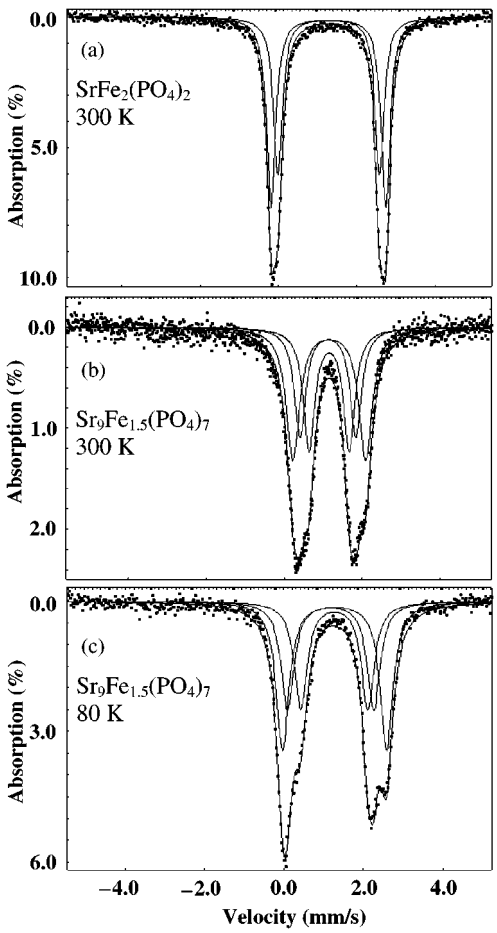

FIG. 1. Mössbauer spectra of (a) $SrFe_2(PO_4)_2$ and (b, c) $Sr_9Fe_{1.5}(PO_4)_7$.

TG and DTG curves for $SrFe_2(PO_4)_2$ and $Sr_9Fe_{1.5}(PO_4)_7$ in air are shown in Fig. 2. $SrFe_2(PO_4)_2$ and $Sr_9Fe_{1.5}(PO_4)_7$ are stable in air up to ~ 750 and ~ 810 K, respectively. The experimental weight gains were 3.98 and 0.75%, which are close to those calculated for $SrFe_2(PO_4)_2$ and $Sr_9Fe_{1.5}(PO_4)_7$, 4.11 and 0.78%, respectively. After oxidation the $Sr_9Fe_{1.5}(PO_4)_7$ specimen contained Fe_2O_3 (2.3 wt%) and $Sr_9Fe(PO_4)_7$ (31). After oxidation the $SrFe_2(PO_4)_2$ specimen contained Fe_2O_3 and unknown phases. The XRD pattern of the obtained unknown phases (after subtraction of reflections of Fe_2O_3) was very close to that of a sample with the total composition $Sr_3Fe_4(PO_4)_6$ obtained from $Sr_3(PO_4)_2$ and $FePO_4$ at 1270 K (100 h).

The magnetic measurements showed that magnetic susceptibility of both samples noticeably depended on the attached magnetic field (Fig. 3). Such behavior usually indicates the presence of traces of ferromagnetic impurities. One can suppose that both samples contained trace quantities of Fe_3O_4 (or Fe), too small to be detected by XRD and Mössbauer spectroscopy. The presence of ferromagnetic impurities in the paramagnetic samples could mask weak

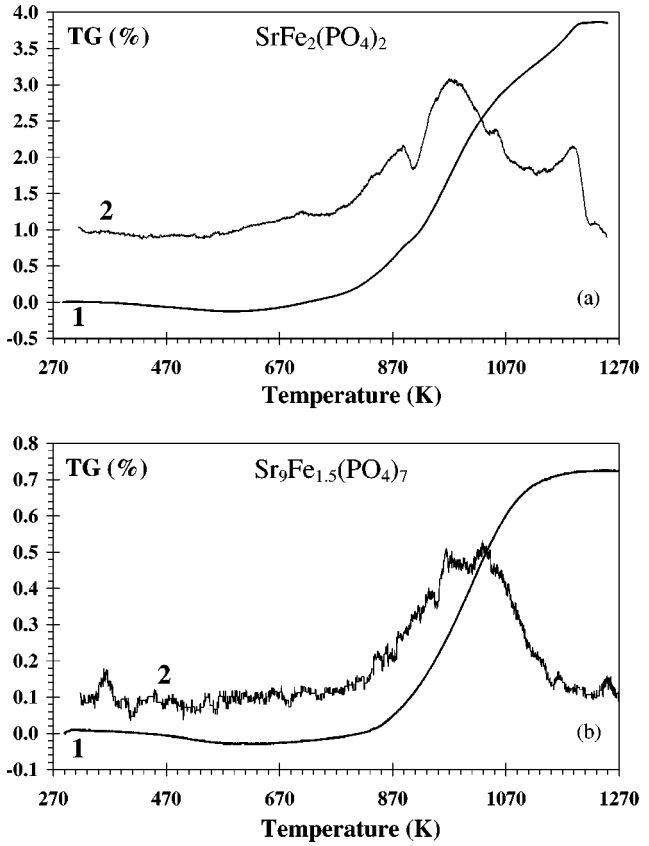

FIG. 2. TG (1) and DTG (2) curves in air for (a) $SrFe_2(PO_4)_2$ and (b) $Sr_9Fe_{1.5}(PO_4)_7$.

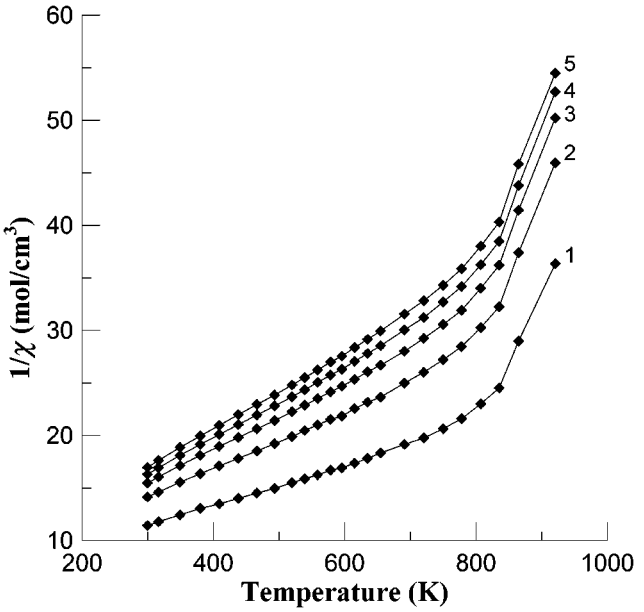

FIG. 3. Temperature dependences of inverse magnetic susceptibility $(1/\chi)$ for $Sr_9Fe_{1.5}(PO_4)_7$. $H = 5950$ Oe (1), 9763 Oe (2), 12045 Oe (3), 13522 Oe (4), and 14779 Oe (5).

effects associated with the oxidation process and makes it impossible to conduct any qualitative deduction from the results of magnetic susceptibility measurements. Nevertheless, the sharp bends in temperature dependence of inverse magnetic susceptibility (Fig. 4) at ~ 730 and ~ 810 K for $SrFe_2(PO_4)_2$ and $Sr_9Fe_{1.5}(PO_4)_7$, respectively, can correspond to the temperatures of the onset of oxidation. These temperatures were close to those obtained by the thermogravimetric method (Fig. 2).

The infrared spectra of $SrFe_2(PO_4)_2$ and $Sr_9Fe_{1.5}(PO_4)_7$ are shown in Fig. 5 and present only P–O stretching and bending bands in a wavenumber range of 500–1300 cm^{-1}. The IR spectrum of $Sr_9Fe_{1.5}(PO_4)_7$ was similar to those of whitlockite-like calcium-containing phosphates (32, 33).

The samples $SrFe_2(PO_4)_2$ and $Sr_9Fe_{1.5}(PO_4)_7$ showed no SHG response, which indicates that the crystal structures of $SrFe_2(PO_4)_2$ and $Sr_9Fe_{1.5}(PO_4)_7$ have a center of symmetry.

3.3. *Crystal Structure Refinement and Description*

The structural data of $Ca_9Cu_{1.5}(PO_4)_7$ (34) were used as an initial model for the structure refinement of $Sr_9Fe_{1.5}(PO_4)_7$. $Ca_9Cu_{1.5}(PO_4)_7$ (space group $R3c$, $a = 10.3379$ Å, $c = 37.1898$ Å, $Z = 6$) is isotypic with β-$Ca_3(PO_4)_2$ and has six cation sites: the distorted octahedral $M5$ site, the eight-coordinated $M1$, $M2$, and $M3$ sites, the half-occupied $M4$ site, and the vacant $M6$ site. The $M4$ and $M6$ sites are the cavities formed by 15 and 10 oxygen atoms, respectively (35). The $M1$–$M3$ sites are in general positions. The $M4$–$M6$ sites lie on a threefold axis. There are three

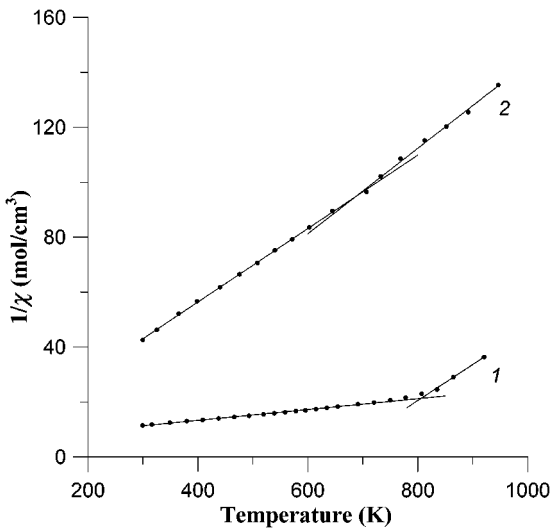

FIG. 4. Temperature dependences of inverse magnetic susceptibility $(1/\chi)$ for (1) $Sr_9Fe_{1.5}(PO_4)_7$ and (2) $SrFe_2(PO_4)_2$ $H = 5950$ Oe.

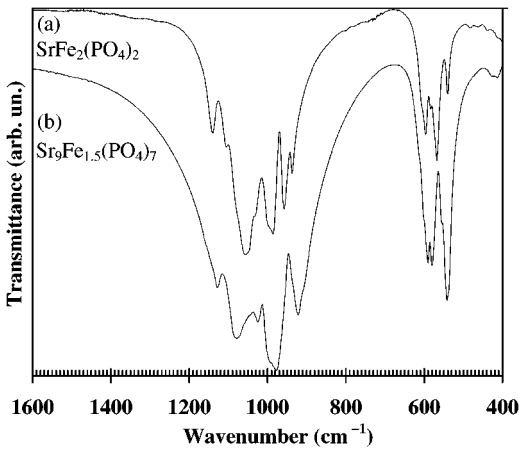

FIG. 5. IR spectra for (a) $SrFe_2(PO_4)_2$ and (b) $Sr_9Fe_{1.5}(PO_4)_7$ in the range 400–1600 cm^{-1}.

phosphorus sites in $Ca_9Cu_{1.5}(PO_4)_7$: P1 is on a threefold axis and P2 and P3 are in general positions. In the initial cation distribution for $Sr_9Fe_{1.5}(PO_4)_7$, strontium cations were placed in the $M1$–$M3$ sites with $n = 1$ (where n is occupancy), iron cations were placed in the $M4$ and $M5$ sites with $n = \frac{1}{2}$ and 1, respectively, and the $M6$ site remained vacant. The refinement in this model gave a good agreement between the experimental and calculated XRD patterns: $R_{wp} = 3.89\%$ ($S = 1.96$), $R_p = 2.88\%$, $R_B = 3.47\%$, $R_F = 2.25\%$. All cations and phosphorus atoms had usual atomic displacement parameters, but most of the oxygen atoms had negative atomic displacement parameters. P–O distances were in the range 1.49–1.68 Å. It was also determined that the oxygen atom O11 had been displaced from the threefold axis (atom O11 on the threefold axis had a very large atomic displacement parameter, $B \approx 400$) and the P1–O11 distance was 1.89 Å.

As SHG studies showed, the structure of $Sr_9Fe_{1.5}(PO_4)_7$ has a center of symmetry, while the structure of $Ca_9Cu_{1.5}(PO_4)_7$ does not. The atomic coordinates of $Sr_9Fe_{1.5}(PO_4)_7$ in the $Ca_9Cu_{1.5}(PO_4)_7$ structure model (space group $R3c$) were transformed to a structure model with space group R–$3c$. In the R–$3c$ structure model the $M1$ and $M2$ sites, the $M4$ and $M6$ sites, the $P2O_4$ and $P3O_4$ tetrahedra are equivalent ($M1 \equiv M2$, $M4 \equiv M6$, P2 ≡ P3, O21 ≡ O34, O22 ≡ O32, O23 ≡ O31, and O24 ≡ O33), the $M5$ site lies at the center of symmetry (site 6*b*), the $M3$ site is located in site 36*f* near the center of symmetry ($\frac{1}{2}, \frac{1}{2}, 0$) (site 18*d*), and the P1 atom is in site 6*a* with coordinates (0, 0, $\frac{1}{4}$). Thus, in the R–$3c$ model the $M3$ and $M4$ sites have $n = \frac{1}{2}$ and $\frac{1}{4}$, respectively. The oxygen atoms around the P1 site were refined as one atom in general position (site 36*f*) with $n = \frac{2}{3}$. (Hereafter, for the structure of $Sr_9Fe_{1.5}(PO_4)_7$ we use the same atom numeration as for $Ca_9Cu_{1.5}(PO_4)_7$ in order to clarify the relationships between positions and crystal structures.) This model gave $R_{wp} = 3.65\%$ ($S = 1.84$), $R_p = 2.78\%$, $R_B = 3.67\%$, $R_F = 2.16\%$. All cations and phosphorus atoms had usual atomic displacement parameters (for example, $B(M3) = 1.65(4)$). All P–O distances were in the range 1.54–1.60 Å. Only one oxygen atom had a negative atomic displacement parameter. Note that when the strontium atom in the $M3$ site was placed in the 18*d* site ($\frac{1}{2}, \frac{1}{2}, 0$), at the center of symmetry, with $n = 1$ the refinement led to $B(M3) = 6.5(1)$ and negative atomic displacement parameters for three oxygen atoms.

All the observed reflections in the $R3c$ and R–$3c$ models (with $a = 10.6102$ Å and $c = 39.427$ Å) had even indexes l. The presence of only even indexes indicated that the c parameter of the unit cell could be reduced by a factor of 2. Indeed, the XRD pattern of $Sr_9Fe_{1.5}(PO_4)_7$ could be indexed in space group R–$3m$ with $a = 10.6102$ Å and $c = 19.7135$ Å. Thus, in the third structure model the atomic coordinates of $Sr_9Fe_{1.5}(PO_4)_7$ in the R–$3c$ space group model were transformed to a structure model with space group R–$3m$ according to a certain cell transformation ($\mathbf{a}' = -\mathbf{a}$, $\mathbf{b}' = -\mathbf{b}$, $2\mathbf{c}' = \mathbf{c}$). In this model the P1 site lies in the 3*b* site (0, 0, $\frac{1}{2}$) at the center of symmetry and strontium atoms in the $M3$ site are located in the 18*h* site near the center of symmetry (site 9*e*) with $n = \frac{1}{2}$. The refinement in the R–$3m$ model gave positive atomic displacement parameters for all atoms and usually observed interatomic distances. We have examined different models of oxygen surrounding the P1 site. The best model was obtained when one oxygen atom was refined in a general position (site 36*i*) with $n = \frac{1}{3}$.

Crystal structure refinement of $Sr_{9.2}Co_{1.3}(PO_4)_7$ (36) from single-crystal data showed that in reality strontium cations in the $M3$ sites are disordered over four positions. Additional splitting of strontium cations in the $M3$ site over two 18*h* sites, $M31$ and $M32$, with $n = \frac{1}{4}$ in the structure of $Sr_9Fe_{1.5}(PO_4)_7$ was successful and led to common $B = 0.47(4)$ and noticeably lower R factors: $R_{wp} = 3.00\%$ ($S = 1.51$), $R_p = 2.35\%$, $R_B = 3.44\%$, $R_F = 1.72\%$, in comparison to when strontium cations were refined in one 18*h* site, $M3$, with $n = \frac{1}{2}$: $R_{wp} = 3.31\%$ ($S = 1.67$), $R_p = 2.58\%$, $R_B = 3.88\%$, $R_F = 2.22\%$, and $B = 1.59(3)$. Table 4 lists experimental/refinement conditions, final R factors, lattice parameters, etc. Final fractional coordinates and atomic displacement parameters are listed in Table 5, and metal–oxygen bond lengths and angles in Table 6. Figure 6 displays observed, calculated, and difference XRD patterns for $Sr_9Fe_{1.5}(PO_4)_7$.

Mössbauer data for $Sr_9Fe_{1.5}(PO_4)_7$ gave evidence of more than two types of iron positions in the structure, while the R–$3m$ (and R–$3c$) structure model has two crystallographically independent iron sites. In order to increase the number of independent sites for iron the unit cell symmetry should be reduced or the unit cell dimensions should be increased. Crystal structure refinements in

TABLE 4
Conditions of the Diffraction Experiments and Parts of the Refinement Results for $Sr_9Fe_{1.5}(PO_4)_7$

Space group	*R*–3*m* (No. 166)
Z	3
2θ range (°)	8–140
Scan step (°)	0.02
I_{max} (counts)	68700
Lattice parameters:	
a (Å)	10.6102(1)
c (Å)	19.7135(1)
V (Å^3)	1921.95(3)
Number of Bragg reflections	480
Variables:	
Structure/lattice	29/2
Background/profiles	10/10
Zero shift/scale	1/1
PPP[a]	41
Reliable factors[b]	
R_{wp}; R_p	3.00% (3.41%); 2.35% (2.61%)
R_B; R_F	3.44% (3.40%); 1.72% (1.77%)
S	1.51 (1.71)

[a] Refined primary profile parameters (PPP).
[b] *R* factors given in parentheses are before applying partial profile relaxation.

TABLE 6
Bond Distances (Å) and Angles (°) for Tetrahedra PO_4^{3-} in $Sr_9Fe_{1.5}(PO_4)_7$

Bonds		Bonds and Angles	
*M*1–O22*2	2.528(3)	*M*31–O22*2	2.514(6)
–O24*2	2.607(2)	–O21*2	2.663(3)
–O22a*2	2.650(2)	–O22a*2	2.607(6)
–O21	2.609(4)	–O21a*2	2.912(3)
–O11*2	2.712(7)	–O11*2	2.893(8)
–O11a*2	2.729(12)	*M*32–O21*2	2.419(3)
*M*4–O21*3	2.362(4)	–O11*2	2.538(8)
–O11*6	2.460(10)	–O22*2	2.577(4)
		–O22a*2	2.699(4)
*M*31–*M*31a[a]	0.422(7)	*M*31–*M*32a[a]	0.862(3)
*M*31–*M*32[a]	0.446(5)	*M*32–*M*32a[a]	1.306(6)
*M*31–*M*4[a]	2.908(4)	*M*32–*M*4[a]	2.483(3)
*M*5–O24*6	2.102(3)	O24–*M*5–O24a	95.2(2)
P1–O11*12	1.536(6)	O21–P2–O22*2	108.3(2)
P2–O21	1.564(4)	O21–P2–O24	112.1(2)
–O22*2	1.555(3)	O22–P2–O22a	113.3(2)
–O24	1.591(3)	O22–P2–O24*2	107.4(2)

Note. Distances for all split O11 positions are given.
[a] Distance between split cation positions.

structure models with more than two types of crystallographically independent iron sites led to worse crystal structure descriptions concerning atomic displacement parameters and some of the P–O and Sr–O distances. Moreover, the XRD pattern of $Sr_9Fe_{1.5}(PO_4)_7$ showed no superstructure reflections and no distortion from the trigonal symmetry. In addition, studies of isotypic centrosymmetric compounds, $Sr_{9.2}Co_{1.3}(PO_4)_7$ (by single-crystal X-ray diffraction) and $Sr_{9.3}Ni_{1.2}(PO_4)_7$ (by neutron powder diffraction and electron microscopy), have confirmed the *R*–3*m* space group with $a \approx 10.6$ Å and $c \approx 19.7$ Å and disordering of $P1O_4^{3-}$ tetrahedra and strontium cations in the *M*3 site. These data will be published elsewhere. Disordering of cations in one position and PO_4^{3-} tetrahedra was also observed in other phosphates, for example, with eulytite structure, $Ba_3Bi(PO_4)_3$ (37) and $Sr_3La(PO_4)_3$ (38).

TABLE 5
Fractional Coordinates and Atomic Displacement Parameters for $Sr_9Fe_{1.5}(PO_4)_7$

Atom[a]	*Site*	*n*	*x*	*y*	*z*	*B* (Å^2)
*M*1	18*h*	1	0.18993(4)	0.81007	0.53794(3)	0.61(2)
*M*31	18*h*	$\frac{1}{4}$	−0.5093(2)	0.5093	0.0063(3)	0.47(4)
*M*32	18*h*	$\frac{1}{4}$	−0.5318(2)	0.5318	0.0148(2)	0.47[b]
*M*4	6*c*	$\frac{1}{4}$	0.0	0.0	0.3550(4)	2.2(2)
*M*5	3*a*	1	0.0	0.0	0.0	0.47(6)
P1	3*b*	1	0.0	0.0	0.5	2.88(14)
P2	18*h*	1	0.49101(9)	0.50899	0.39797(12)	0.80(4)
O11	36*i*	$\frac{1}{3}$	0.8989(11)	0.0380(12)	0.5398(4)	3.8(3)
O21	18*h*	1	0.5388(2)	0.4612	0.6764(2)	1.42(11)
O22	36*i*	1	0.2625(3)	0.0087(2)	0.23304(14)	0.34(6)
O24	18*h*	1	0.9109(2)	0.0891	0.0669(2)	0.23(9)

Note. Atom numeration is retained as that in $Ca_9Cu_{1.5}(PO_4)_7$ (34).
[a] The *M*1, *M*31, and *M*32 sites are occupied by Sr^{2+}; the *M*4 and *M*5 sites are occupied by Fe^{2+}.
[b] Atomic displacement parameters for the *M*31 and *M*32 sites were constrained.

Some contradictions between the crystal structure refinement and Mössbauer data for $Sr_9Fe_{1.5}(PO_4)_7$ may be explained by the following. In order to maintain the local center of symmetry in the *M*5 sites the structure should contain fragments $\cdots$–$P1O_4$–*M*4O_n–*M*5O_6–*M*4O_n–$P1O_4$–$\cdots$ where both *M*4 sites are occupied by iron cations or vacant. Thus, the *M*5 site may have a different environment. Disordering of these fragments gives an average structure detected by XRD, while Mössbauer data give information about the local environment of iron cations. In addition, the oxygen environment of iron cations in the *M*4 sites depends on the orientation of the disordered $P1O_4^{3-}$ tetrahedra.

The structure of $Sr_9Fe_{1.5}(PO_4)_7$ is related to β-$Ca_3(PO_4)_2$ (26) and α-$Sr_3(PO_4)_2$ (space group *R*–3*m*, $a = 5.3901$ Å, $c = 19.785$ Å, $Z = 3$) (28). The compound $Sr_9Fe_{1.5}(PO_4)_7$ has a doubled *a* axis in comparison with α-$Sr_3(PO_4)_2$, and β-$Ca_3(PO_4)_2$ has a doubled *c* axis in comparison with $Sr_9Fe_{1.5}(PO_4)_7$. Projections of these three structures viewed along the [001] and [110] directions are shown in Figs. 7 and 8. The structure of α-$Sr_3(PO_4)_2$ can be constructed from

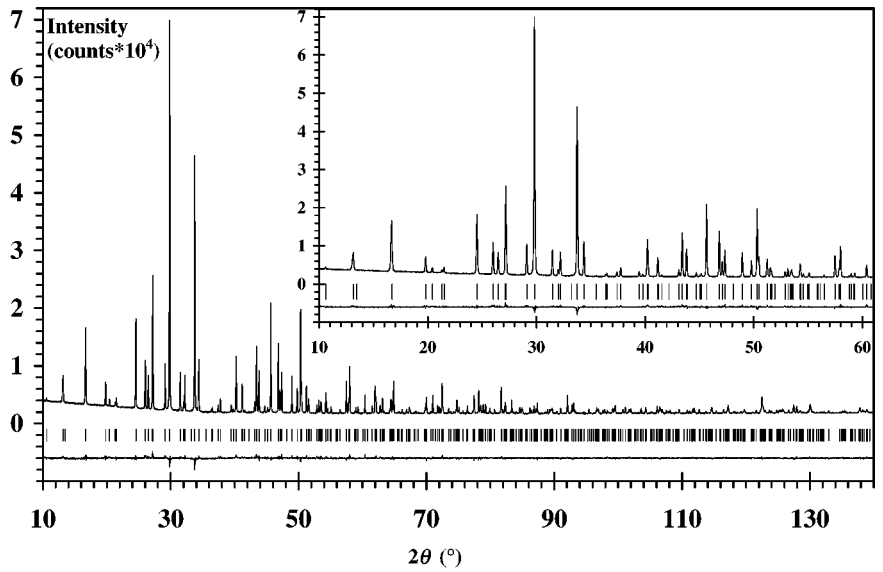

FIG. 6. Experimental, calculated, and difference XRD patterns for $Sr_9Fe_{1.5}(PO_4)_7$. Bragg reflections are marked by short bars. The inset shows a portion of the Rietveld refinement profiles.

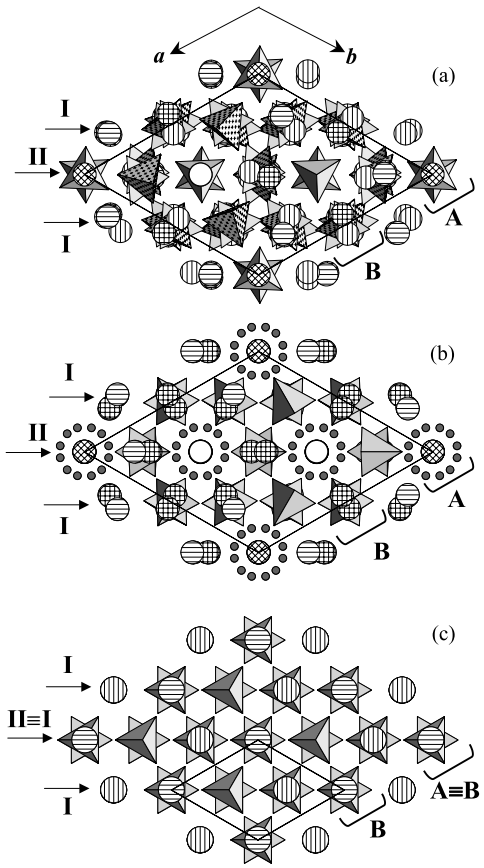

FIG. 7. Crystal structures of (a) β-$Ca_3(PO_4)_2$, (b) $Sr_9Fe_{1.5}(PO_4)_7$, and (c) α-$Sr_3(PO_4)_2$ viewed along the [001] direction. Layers I and II, and columns *A* and *B* are marked. Unit cells of the three structures are shown. The split O11 (small dark circles) and *M*3 positions are shown for the structure of $Sr_9Fe_{1.5}(PO_4)_7$.

one type of layers, I. Layer I contains one type of columns, *B*. The structures of $Sr_9Fe_{1.5}(PO_4)_7$ and β-$Ca_3(PO_4)_2$ can be constructed from two types of layers I and II (35). Layer I contains columns *B*, while layer II contains columns *A* and *B*. Layer I and column *B* are very similar in these three structures (Fig. 8). The main difference among the three structures is in layer II and column *A* (Fig. 8). Column *A* in $Sr_9Fe_{1.5}(PO_4)_7$ differs from that in α-$Sr_3(PO_4)_2$ ($A \equiv B$) by elimination of one PO_4 tetrahedron, orientation disordering of another PO_4 tetrahedron, and change of site occupancies from 1 (Sr2 in α-$Sr_3(PO_4)_2$) to $\frac{1}{4}$ (*M*4 in $Sr_9Fe_{1.5}(PO_4)_7$) in order to compensate the PO_4^{3-} tetrahedra elimination (Figs. 8b, 8c). Column *A* in β-$Ca_3(PO_4)_2$ differs from that in $Sr_9Fe_{1.5}(PO_4)_7$ by orientation ordering of $P1O_4$ tetrahedra and ordering of occupancies of the *M*4 and *M*6 sites ($n = \frac{1}{2}$ and 0, respectively) (Figs. 8a, 8b). The possible reason of disordering in the structure of $Sr_9Fe_{1.5}(PO_4)_7$ is the following. Simultaneous occupation of the *M*4 and *M*6 sites should result in the displacement of the O11 and *M*3 atoms because the distances $d(M3–M6) \sim 2.5$ Å and $d(O11–M6) \sim 0.5$ Å are too short in the structure of β-$Ca_3(PO_4)_2$ (if $z_{M6} = -z_{M4}$) (Fig. 8a). Occupancy of the *M*4 site is equal to $\frac{1}{4}$ in $Sr_9Fe_{1.5}(PO_4)_7$, so the positions of the O11 and *M*3 atoms depend on whether the *M*4 site is occupied or vacant. In the obtained model (space group *R*–3*m*) of the crystal structure of $Sr_9Fe_{1.5}(PO_4)_7$, the P1 atom lies at the center of symmetry, which just reflects the disordering of oxygen surrounding the P1 atom. One can see from Fig. 8a that if in the structure of β-$Ca_3(PO_4)_2$ the *M*4 and *M*6 sites become equivalent and the O11 atoms in the $P1O_4$ tetahedra are displaced from the threefold axis, then, formally, the *c* parameter may be reduced by a factor

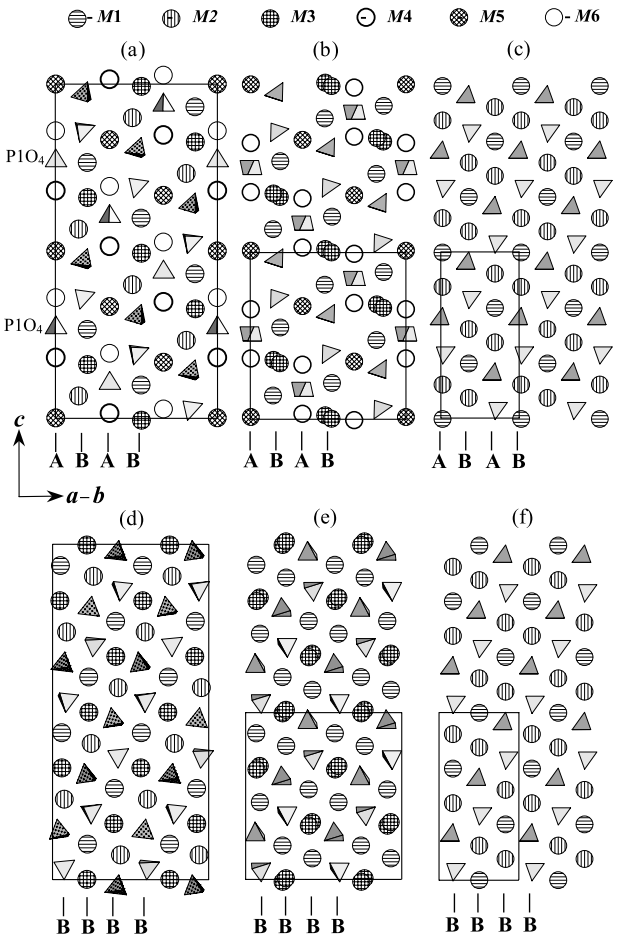

FIG. 8. Layer II (a, b, c) and layer I (d, e, f) in the crystal structures of (a, d) β-$Ca_3(PO_4)_2$, (b, e) $Sr_9Fe_{1.5}(PO_4)_7$, and (c, f) α-$Sr_3(PO_4)_2$ viewed along the [110] direction. Columns *A* and *B* are marked. Unit cells of the three structures are shown. The disordered $P1O_4$ tetrahedra and the split *M*3 positions are shown for the structure of $Sr_9Fe_{1.5}(PO_4)_7$.

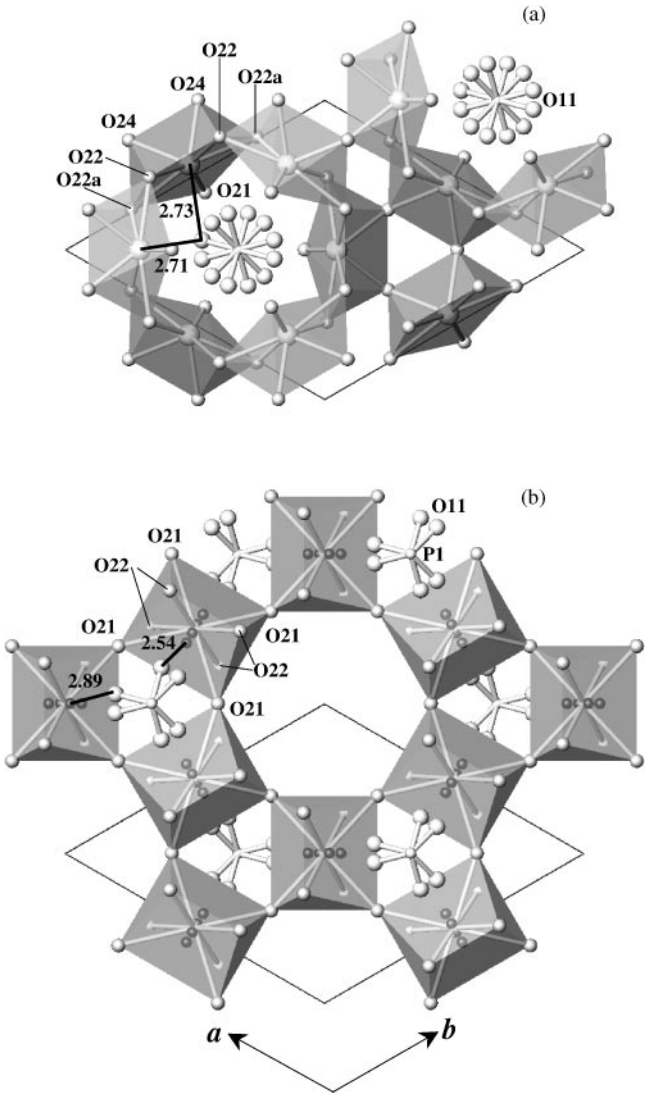

FIG. 9. Polyhedra for (a) the *M*1 sites and (b) the ideal *M*3 sites (that is, in site 9*e*) without O11 atoms viewed along the [001] direction. Split O11 atoms are shown by circles bonded to the P1 atoms. The *M*31 and *M*32 sites are shown by small dark circles inside transparent polyhedra. Interatomic distances are given in angstroms.

of 2. The structure of $Sr_9Fe_{1.5}(PO_4)_7$ may be considered as the intermediate structure between β-$Ca_3(PO_4)_2$ and α-$Sr_3(PO_4)_2$. However, the structure of $Sr_9Fe_{1.5}(PO_4)_7$ is topologically more similar to that of β-$Ca_3(PO_4)_2$, because they differ by different site occupancies and by different tetrahedra orientations, while the difference between α-$Sr_3(PO_4)_2$ and $Sr_9Fe_{1.5}(PO_4)_7$ involves the elimination of tetrahedra.

Polyhedra without the O11 atoms for the *M*1 sites and for the ideal *M*3 sites (that is, in site 9*e*) are shown in Fig. 9. Table 6 gives interatomic distances for all split O11 atoms. Independent of the $P1O_4$ tetrahedra orientation the *M*1 sites have coordination number 8 (Fig. 9a), as in other β-$Ca_3(PO_4)_2$-related compounds (32–34). The coordination number for the *M*31 and *M*32 sites can change, depending on the $P1O_4$ tetrahedra orientation: 8 or 9 for the *M*31 sites and 6 or 7 for the *M*32 sites.

ACKNOWLEDGMENTS

This work was supported by the Russian Foundation for Basic Research (Grants 00-03-32660 and 01-03-06122). The authors thank Dr. S.S. Khasanov (Institute of Solid State Physics, Russia) for XRD measurements and Dr. S.Yu. Stefanovich (Moscow State University) for SHG study.

REFERENCES

1. J. F. Sarver, M. V. Hoffman, and F. A. Hummel, *J. Electrochem. Soc.* **108,** 1103 (1961).
2. J. R. Looney and J. J. Brown, *J. Electrochem. Soc.* **118,** 470 (1971).
3. H. Koelmans and A. P. M. Cox, *J. Electrochem. Soc.* **104,** 442 (1957).

4. H. Donker, W. M. A. Smit, and G. Blasse, *J. Electrochem. Soc.* **136,** 3130 (1989).
5. V. Pelova, K. Kynev, and G. Gochev, *J. Mater. Sci. Lett.* **14,** 330 (1995).
6. A. Hemon and G. Courbion, *J. Solid State Chem.* **85,** 164 (1990).
7. B. Elbali, A. Boukhari, J. Aride, and F. Abraham, *J. Solid State Chem.* **104,** 453–459 (1993), doi:10.1006/jssc.1993.1180.
8. B. Elbali and A. Boukhari, *Acta Crystallogr. Sect. C* **49,** 1131 (1993).
9. B. Elbali, A. Boukhari, E. M. Holt, and J. Aride, *J. Crystallogr. Spectrosc. Res.* **23,** 1001 (1993).
10. A. A. Belik, B. I. Lazoryak, T. P. Terekhina, and S. N. Polyakov, *Russ. J. Inorg. Chem.* **46**(9), 1312 (2001).
11. B. El-Bali, A. Boukhari, R. Glaum, M. Gerk, and K. Maass, *Z. Anorg. Allg. Chem.* **626,** 2557 (2000).
12. H. Effenberger, *J. Solid State Chem.* **142,** 6 (1999), doi:10.1006/jssc.1998.7953.
13. A. A. Belik, A. P. Malakho, B. I. Lazoryak, and S. S. Khasanov, *J. Solid State Chem.*, doi: 10.1006/jssc.2001.9380.
14. M. B. Korzenski, J. W. Kolis, and G. J. Long, *J. Solid State Chem.* **147,** 390 (1999), doi:10.1006/jssc.1999.8392.
15. K.-H. Lii, P.-F. Shin, and T.-M. Chen, *Inorg. Chem.* **32,** 4373 (1993).
16. A. Boutfessi, A. Boukhari, and E. M. Holt, *Acta Crystallogr. Sect. C.* **51,** 346 (1995).
17. J.-M. Le Meins and G. Courbion, *Acta Crystallogr. Sect. C* **55,** 481 (1999).
18. K.-H. Lii, T.-Y. Dong, C.-Y. Cheng, and S.-L. Wang, *J. Chem. Soc. Dalton Trans.* 577 (1993).
19. K.-H. Lii, T.-S. Lee, S.-N. Liu, and S.-L. Wang, *J. Chem. Soc. Dalton Trans.* 1051 (1993).
20. H. M. Rietveld, *Acta Crystallogr.* **22,** 151 (1967).
21. F. Izumi and T. Ikeda, *Mater. Sci. Forum* **321–324,** 198 (2000).
22. F. Izumi, *Rigaku J.* **17,** 34 (2000).
23. H. Toraya, *J. Appl. Crystallogr.* **23,** 485 (1990).
24. "International Tables for Crystallography," Vol. C, p. 500, Kluwer, Dordrecht, 1992.
25. P. E. Warner, L. Eriksson, and M. Westdahl, *J. Appl. Crystallogr.* **18,** 367 (1985).
26. B. Dickens, L. W. Schroeder, and W. E. Brown, *J. Solid State Chem.* **10,** 232 (1974).
27. C. Calvo and R. Gopal, *Am. Miner.* **60,** 120 (1975).
28. K. Sugujama and M. Tokonami, *Mineral J.* **15,** 141 (1990).
29. A. A. Belik, A. P. Malakho, B. I. Lazoryak, and S. S. Khasanov, submitted.
30. F. Menil, *J. Phys. Chem. Solids.* **46,** 763 (1985).
31. A. A. Belik, F. Izumi, T. Ikeda, M. Okvi, A. P. Malakho, and B. I. Lazoryak, in preparation.
32. B. I. Lazoryak, V. A. Morozov, A. A. Belik, S. S. Khasanov, V. Sh. Shekhtman, *J. Solid State Chem.* **122,** 15 (1996), doi:10.1006/jssc.1996.0074.
33. B. I. Lazoryak, N. Khan, V. A. Morozov, A. A. Belik, and S. S. Khasanov, *J. Solid State Chem.* **145,** 345 (1999), (doi:10.1006/jssc.1999.8294).
34. A. A. Belik, O. V. Yanov, and B. I. Lazoryak, *Mater. Res. Bull.* **36,** 1863 (2001).
35. B. I. Lazoryak, *Russ. Chem. Rev.* **65,** 287 (1996).
36. A. A. Belik and B. I. Lazoryak, unpublished results.
37. E. H. Arbib, B. Elouadi, J. P. Chaminade, and J. Darriet, *Mater. Res. Bull.* **35,** 761 (2000).
38. J. Barbier, J. E. Greedan, T. Asaro, and G. J. McCarthy, *Eur. J. Solid State Inorg. Chem.* **27,** 855 (1990).